Turbulent transport in wall subchannels and in finite rod clusters

K. M. Sahoo and A. K. Mohanty
Department of Mechanical Engineering, Indian Institute of Technology, Kharagpur, India

Turbulent transport through wall subchannels of circular and hexagonal rod clusters has been studied using a two-dimensional eddy diffusivity. Fully developed flow and thermal conditions are assumed, and finite-difference solutions have been generated for the uniform heat flux condition on the rod surface. Transport rate values are estimated for subchannels with curved as well as straight boundaries with the pitch-to-diameter and wall-to-diameter ratios varying over a wide range. The cluster-average transport coefficients are next generated for circular bundles by suitably combining the results for constituent subchannels. Quantitative agreement with experimental results in the literature are attained. The accuracy of turbulence modeling is attested to by the fact that the cluster-average friction factor and Nusselt number values are in reasonable agreement with the well-established internal flow correlations based on hydraulic diameter.

Keywords: rod cluster; turbulence; wall subchannel; 2-D eddy diffusivity

Introduction

Thermal hydraulic studies relating to the safety of a nuclear reactor have assumed considerable significance in recent years in the wake of the Three Mile Island (TMI)-2 and the Chernobyl accidents. In the event of a loss-of-coolant accident, the degeneration in coolant flow rate through the calandria results in reduced heat transfer and consequent overheating of the rod surface that leads to oxidation of the cladding and possibly to a meltdown of the core. The postulated sequence of events points to the need of a knowledge of transport rate values for individual rods under laminar and low turbulent flow conditions. In evaluating the single-rod related values, the calandria geometry is modeled in either of two methods: triangular or square subchannels, and symmetry sectors. The latter approach is pertinent to small reactors, such as those of the CANDU design. A symmetry sector is multiply connected, and turbulence modeling for the complex geometry is formidable. In an earlier work, the present authors proposed a method of superposition[1] wherein results of constituent subchannels (see Figure 1) could be suitably combined to generate the cluster average transport rate values in the laminar regime. The exercise corroborated the propositions of Rehme.[2] The superposition method could, logically be attempted for turbulence modeling in a finite bundle.

The symmetry sector can be discretized into a number of interior and wall subchannels. The results for turbulent flow through interior subchannels were reported by Mohanty and Sahoo.[3] The present article is aimed at the evaluation of transport rate values for the wall subchannels, as a complement to the earlier work.[3]

Rods near a bounding wall, i.e., in a wall subchannel, have been shown to be overheated for the wall-to-diameter ratio in the neighborhood of 1.4 as compared to their counterparts in the interior, even under no power-skew condition.[4] Buoyancy and back-flow effects become prominent near a bounding wall. The wall subchannels have attracted both analytical and experimental investigations by Rehme,[5,6] Seale,[7–9] and Slagter,[10] among others. Studies by Seale and Slagter included effects of secondary flow and anisotropic eddy viscosity.

Algebraic mixing length as well as higher-order closure models have been used to model turbulence in rod-bundle geometries. Buleev's mixing length was used by Ramm and Johannsen[11] and Slagter,[10] whereas Prandtl's mixing length was adopted by Meyder[12] and Thompson and Holy.[13] Deviations of computed results from experiments were generally attributed to anisotropic eddy diffusivities.

A one-equation (k–1) model was adopted by Carajilescov and Todreas[14] and Trupp and Aly.[15] Batzis and Todreas[16] also applied a k–ε model. These closure models were generally oriented towards assessing the effects of secondary flow. Batzis and Todreas[16] found it to be less than 1% of the axial flow. Seale[8] remarked that secondary flow, even in conjunction with large anisotropic diffusivity, has only a marginal effect on heat transfer. The anisotropy factor is defined as $\psi = \varepsilon_{m\theta}/\varepsilon_{mr}$, where θ and r are the angular and radial directions. $\varepsilon_{m\theta}$ is experimentally estimated by dividing the measured peripheral Reynolds stress by the velocity gradient in the θ-direction. It is a common experience that, even in low PDR arrangements, the peripheral velocity gradients are orders of magnitude lower than the radial gradient, leaving a scope for inaccuracy in experimental estimation. As a result, a common practice in the literature has been to examine the effects of anisotropy through parametric variation of ψ (see Trupp and Aly[15]). Bartzis and Todreas[16] expressed ψ as a ratio of length scales, and Rehme[17] observed it to be a point function that varied radially in a wall subchannel.

A general observation is that variations of ψ do not substantially change the transport rate values but do flatten the wall shear stress and temperature distributions (see Thompson and Holy[13] and Rapley[18]). This observation was corroborated by the present authors in a study of the interior subchannels[3] through an anisotropic k–1 formulation.

The thrust of the thermal-hydraulic studies pertains to reactor safety considerations. Since it is observed that anisotropy or secondary flow reduces the rod surface temperature variation, uncertainties in their values or model can inadvertently lead to

Address reprint requests to Professor Mohanty at the Department of Mechanical Engineering, Indian Institute of Technology, Kharagpur, India.

Received 8 June 1990; accepted 17 December 1990

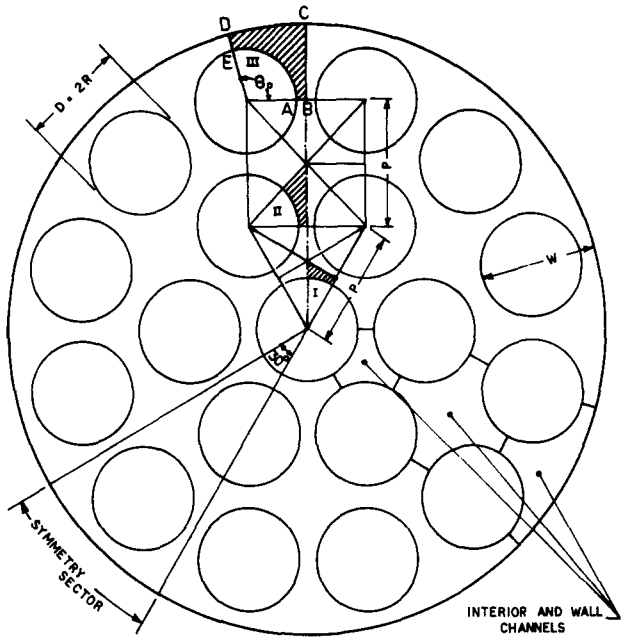

Figure 1 Nineteen-rod circular cluster showing the various subchannels

underprediction of the hot-spot temperature, signaling lack of prudence regarding safety considerations.

Given the above background, we proposed a two-dimensional (2-D) eddy diffusivity,[3] without the inclusion of secondary flow or anisotropy, for subchannel analysis.

The 2-D model is here applied to wall subchannels of circular and hexagonal shells. The accuracy of the results so derived is established through a process of integration: (1) the wall subchannel average transport rate values are combined with those for the interior subchannels of ref. 3, following the procedure enumerated in ref. 1; and (2) the bundle average values so constructed are compared with experimental results in the literature. Agreement of the friction factor in a circular bundle to better than 10% lends confidence to this study.

Analysis

Physical model

The rod-bundle geometry in a circular shell is divided into subchannel types I, II, and III as shown in Figure 1. Type III is the geometry of present interest. An enlarged view is presented in Figure 2. While AOE is a sector of the fuel rod, CD is a portion of the shell surface. The included angle θ_0 is given by $\theta_0 = \pi(0.5 + 1/N)$, where N is the number of rods in the outermost row of the cluster. For a straight-boundary wall subchannel, type IV, which belongs to a square or a hexagonal cluster, θ_0 is always 90°. The domain of computation is bounded by symmetry lines AB, BC, and DE, across which the normal gradient of a parameter is taken as zero. The velocity is zero on the solid surfaces AE and CD. Thermal solutions are obtained for a uniform heat flux condition on the rod surface, and the shell wall CD is treated adiabatic.

The 2-D diffusivity,[3] conceived in the model of Reichardt's eddy viscosity, requires an a priori identification of the line of zero shear stress, on which the velocity may also be considered

Notation

A	Flow area, $A^* = A/R^2$
C_p	Fluid specific heat at constant pressure
D	Rod diameter
D_h	Hydraulic diameter, $D_h^* = D_h/R$
f	Fanning's friction factor
G_m	Source term for momentum equation
h	Heat transfer coefficient
k	Mixing length coefficient
k_1	Molecular thermal conductivity
k_t	Turbulent thermal conductivity
l	Length scale of turbulence
MVL	Maximum velocity line
Nu	Nusselt number, $\mathrm{Nu} = hD_h/k_1$
P	Pitch, distance between two adjacent rod centers
P/D	Pitch-to-diameter ratio
P_h	Heated perimeter, $P_h = P_h^*/R$
$\frac{dp}{dz}$	Axial pressure gradient
Pr	Prandtl number
Pr_t	Turbulent Prandtl number, $\mathrm{Pr}_t = \varepsilon_m/\varepsilon_h$
q	Heat flux on rod surface
R	Rod radius
r	Radial distance, $r^* = r/R$
$\hat{r}(\theta)$	Radial distance of the MVL from the rod center
Re	Reynolds number
Re_t	Turbulent Reynolds number, $\mathrm{Re}_t = \bar{u}^+ R/\nu$
St	Stanton number, $\mathrm{St} = q/[\rho C_p \bar{u}(T_w - T_b)]$
S	Distance measured along the shell wall from point C of a straight boundary wall subchannel
T	Temperature, $T^* = T/T_{\mathrm{ref}}$
T_w	Temperature on rod surface
T_b	Bulk temperature of fluid
T_{ref}	Reference temperature, $T_{\mathrm{ref}} = qR/k_1$
u	Axial velocity, $u^* = u/\bar{u}^+$
u^+	Friction velocity, $u^+ = \sqrt{\tau_w/\rho}$
y	Radial distance measured from solid surface, $y^* = y/R$
$\hat{y}(\theta)$	Maximum value of y at the MVL
y^+	Nondimensional distance from the wall, $y^+ = yu^+/\nu$

Greek symbols

α	Thermal diffusivity
ε_m	Eddy diffusivity of momentum, $\varepsilon_{\mathrm{em}} = (1 + \varepsilon_m/\nu)$
ε_h	Eddy diffusivity of heat, $\varepsilon_{\mathrm{eh}} = (\mathrm{Pr}_t/\mathrm{Pr} + \varepsilon_m/\nu)$
ρ	Density
μ	Dynamic viscosity
ν	Kinematic viscosity
τ_w	Wall shear stress
θ	Angular coordinate
θ_0	Total included angle of a subchannel

Superscripts

$-$	Average
$*$	Nondimensional

Subscripts

c	Cluster-average values
i	Inner
o	Outer

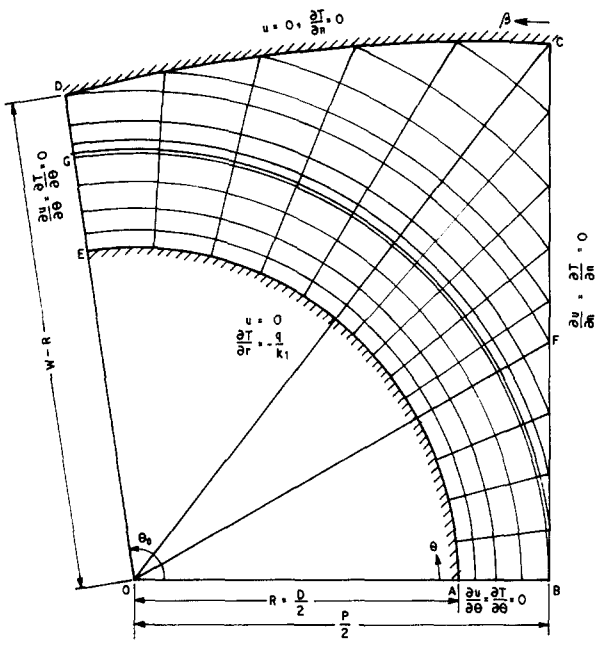

Figure 2 Sample mesh and boundary conditions of a typical wall subchannel, Type III

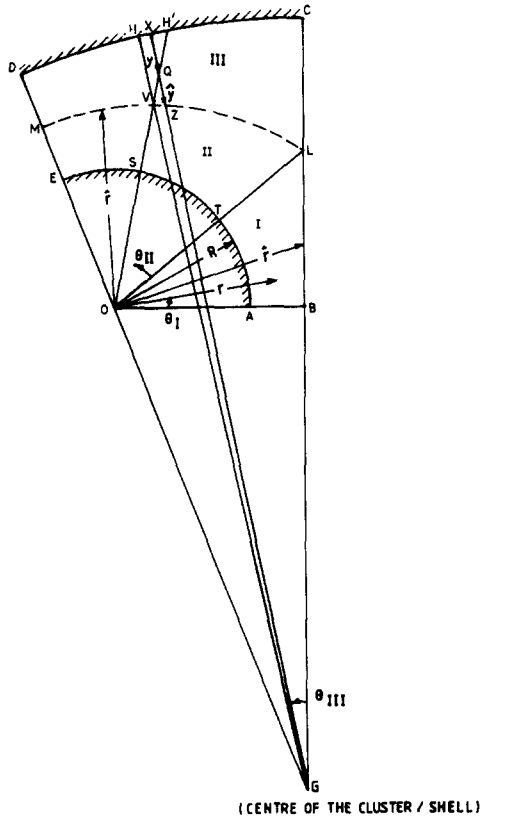

Figure 3 Determination of equidistant line

to have attained its locally maximum values (MVL). In Figure 3, the dotted curve is postulated to represent the MVL. This curve has been drawn, guided by the experience of the laminar flow in ref. 1, as equidistant from the shell surface CD and the rod surface EA. From a point V on the MVL, VS = VH, the two being respective normals to the solid surfaces.

The domain of computation is divided into three zones (see Figure 3). Zone I, ABLT, is similar to a triangular subchannel. Zone II spreads between the rod surface and the MVL. Zone III constitutes the region beyond the MVL up to the shell surface. In zone III the computation is carried out along VH'—an extension of the radial line OSV. The perpendicular distance of a point Q from the shell surface is QX, measured along a radius GX.

Governing equations

For a fully developed, constant property flow of an incompressible fluid, the axial momentum and energy equations are written as

$$\nabla\cdot\left[\left(1+\frac{\varepsilon_m}{\nu}\right)\nabla u\right]=\frac{1}{\mu}\frac{dp}{dz} \tag{1}$$

$$\nabla\cdot\left[\left(1+\frac{k_t}{k_1}\right)\nabla T\right]=\frac{u}{\alpha}\frac{\partial T}{\partial z} \tag{2}$$

The pressure gradient and the subchannel average shear stress, wetted over the rod and shell surfaces taken together, are related as

$$-\frac{dp}{dz}=\frac{4\bar{\tau}_w}{D_h}=\frac{4\rho\bar{u}^{+2}}{D_h} \tag{3}$$

Nondimensionalizing the velocity through $\bar{u}^+$ and radial distance through R, the momentum equation is written as below.

$$\nabla[\varepsilon_{em}\nabla\bar{u}^+]=\frac{1}{\mu}\frac{dp}{dz}\frac{R^2}{\bar{u}^+} \tag{4}$$

Further, we can write the right-hand side of Equation 4 as

$$G_m=\frac{1}{\mu}\frac{dp}{dz}\frac{R^2}{\bar{u}^+}=-\frac{4\mathrm{Re}_t}{D_h^*} \tag{5}$$

in terms of a turbulent Reynolds number Re_t. For a fully developed thermal condition

$$\frac{\partial T}{\partial z}=\frac{dT_b}{dz}=\frac{qP_h}{\rho C_p\bar{u}A} \tag{6}$$

Substitution of Equation 6 into Equation 2 together with the definition of eddy diffusivity of heat $\varepsilon_h=k_t/\rho c_p$ and the turbulent Prandtl number $\mathrm{Pr}_t=\varepsilon_m/\varepsilon_h$ leads to

$$\nabla\cdot(\varepsilon_{eh}\nabla T^*)=\frac{u^*\mathrm{Pr}_tP_h^*}{\bar{u}^*\mathrm{Pr}A^*} \tag{7}$$

where the temperature is normalized as $T^*=T/T_{\mathrm{ref}}$ with $T_{\mathrm{ref}}=qR/k_1$. Solution of Equations 4 and 7 subject to the boundary conditions indicated on Figure 2 yields the velocity and temperature fields.

Two-dimensional diffusivity

The Richardt's eddy diffusivity for zones I and II is written in the manner for a triangular subchannel (see Mohanty and Sahoo[3])

$$\frac{\varepsilon_m(r,\theta)}{\nu}=\frac{\bar{k}_i}{6}[\hat{r}(\theta)-R]\sqrt{\frac{\tau_w(\theta)/\rho}{\nu}}\left[1-\left(\frac{\hat{r}(\theta)-r}{\hat{r}(\theta)-R}\right)^2\right]\times\left[1+2\left(\frac{\hat{r}(\theta)-r}{\hat{r}(\theta)-R}\right)^2\right] \tag{8}$$

In zone III, for a point Q, XZ = $\hat{y}$ and XQ = y, the perpendicular distances measured along the radius drawn from the shell-center G. In terms of y and $\hat{y}$, the eddy diffusivity is written for zone

III as

$$\frac{\varepsilon_m(y,\theta)}{\nu}=\frac{\bar{k}_i}{6}\hat{y}(\theta)\sqrt{\frac{\tau_w(\theta)/\rho}{\nu}}\left[1-\left(\frac{\hat{y}(\theta)-y}{\hat{y}(\theta)}\right)^2\right]\times\left[1+2\left(\frac{\hat{y}(\theta)-y}{\hat{y}(\theta)}\right)^2\right] \tag{9}$$

the average value of $\bar{k}_1$ in Equation 8 was taken as 0.5 based on an exercise for the inner region of an annulus (see ref. 19). $\bar{k}$ for zone III was maintained as 0.4.

Method of solution

Equations 4 and 7 were solved by finite-difference methods for different input values of Re_t and appropriate values of Pr_t and Pr for various subchannel dimensions. A central difference scheme based on the method of Taylor's series was adopted. A sample grid is shown in Figure 2 for a curved-boundary wall subchannel. The distance AB was divided according to a geometric progression so as to have closer grid points near the rod surface. The mesh was also nonuniform in the θ-direction with the objective being to locate the peripheral nodes on the boundary of the computational domain. The turbulence equations were solved from the second string of nodes, counted from the rod and shell wall. These nodes were made to lie beyond the laminar sublayer, i.e., $y^+ \geq 30$. The wall function used for velocity near a solid surface is given by the law of the wall:

$$u_2(\theta)=\sqrt{\frac{\tau_w(\theta)}{\rho}}\left(\frac{1}{k}\ln y_2^+ + C\right) \tag{10}$$

The constants k and C were such that $u/u^+=14.84$ at $y^+=42$ using the suggestions of Levy[20] for an annulus. At the end of each cycle of iteration, the local values of τ_w were updated using the improved values of u_3 from the third row. The distribution of ε_m was obtained by Equations 8 and 9.

The temperature on the rod surface, subjected to a uniform heat flux condition, was estimated using the Stanton number relationship of Jayatilake:[21]

$$\mathrm{St}=\frac{u^+/u}{\mathrm{Pr}_t\left(P_T+\dfrac{u}{u^+}\right)} \tag{11}$$

where P_T, the resistance to the laminar sublayer, is given by

$$P_T=9.24\left[\left(\frac{\mathrm{Pr}}{\mathrm{Pr}_t}\right)^{0.75}-1\right]\times[1+0.29\exp(-0.007\,\mathrm{Pr}/\mathrm{Pr}_t)] \tag{12}$$

In order to choose an appropriate value or function for the turbulence Prandtl number, several sets of calculations were made for annuli of different radius ratio and interior subchannels in ref. 3. It was found that the Wassel and Catton[22] expression for Pr_t is more generally applicable. The expression of ref. 22 has been chosen for the wall subchannels:

$$\mathrm{Pr}_t=\frac{C_3}{C_1\mathrm{Pr}}\frac{[1-\exp\{-C_4/(\varepsilon_m/\nu)\}]}{[1-\exp\{-C_2/\mathrm{Pr}(\varepsilon_m/\nu)\}]} \tag{13}$$

The values of the constants C_1, C_2, C_3, and C_4 are, respectively, 0.21, 5.25, 0.20, and 5.0.

The difference equations were solved iteratively with a relaxation factor varying between 1.3 and 1.5. Velocity and temperature gradients on the orthogonally intersected boundary AB and DE were satisfied through a quadratic polynomial. A six-point interpolation scheme (Mohanty and Sahoo[1]) was applied to treat the conditions on the nonorthogonally intersected nodes on BC and CD (see Figure 2).

Fanning's friction factor f follows from Equation 3 as

$$f=\frac{2.0}{(\bar{u}^+)^2} \tag{14}$$

The Nusselt number based on the average temperature of the rod surface and of the bulk fluid is

$$\mathrm{Nu}=\frac{D_h^*}{\bar{T}_w^*-T_b^*} \tag{15}$$

The velocity and temperature distribution in the flow field were utilized to evaluate the transport parameters following Equations 14 and 15.

Superposition

The transport rates for a finite bundle are evaluated by suitably combining the results for the constituent subchannels. The combination or superposition is carried out because (1) the cluster-average flow rate is equal to the sum of the subchannel flow rates; (2) the pressure gradient is uniform on all the constituent subchannels; and (3) the pressure gradient is balanced by the wall shear stress in a fully developed flow.

The source term for momentum equation is given by Equation 5. But since

$$\mathrm{Re}_t=\frac{R}{\nu}\sqrt{\frac{\bar{\tau}_w}{\rho}} \quad \text{and} \quad \bar{\tau}_w=\left(-\frac{dp}{dz}\right)\frac{D_h}{4},$$

the input parameter Re_t varies from subchannel to subchannel as D_h varies. The solution for a subchannel i (see Figure 1) is carried out by choosing the Re_{t_i} values as

$$\frac{\mathrm{Re}_{t_i}}{\mathrm{Re}_{t_{\mathrm{ref}}}}=\sqrt{\frac{D_{h_i}}{D_{h_{\mathrm{ref}}}}} \tag{16}$$

where the reference subchannel could be chosen from the constituents (see Figure 1). Equation 16, in effect, ensures imposition of the same value of the pressure gradient on all subchannels. Furthermore, for fully developed flow

$$-\frac{dp}{dz}=\frac{\bar{\tau}_{w1}P_{w1}}{A_1}=\frac{\bar{\tau}_{w2}P_{w2}}{A_2}=\ldots=\frac{\bar{\tau}_{wc}P_{wc}}{A_c} \tag{17}$$

and the definition of Fanning's friction factor

$$(f\mathrm{Re})_i=\frac{\bar{\tau}_{wi}P_{wi}D_{hi}^2}{2\nu m_i} \tag{18}$$

leads to

$$(f\mathrm{Re})_1\frac{\dot{m}_1}{A_1D_{h1}^2}=-\frac{1}{2\nu}\frac{dp}{dz}=(f\mathrm{Re})\frac{\dot{m}_2}{A_2D_{h2}^2}\ldots=(f\mathrm{Re})_c\frac{\dot{m}_c}{A_cD_{hc}^2} \tag{19}$$

The conservation of mass yields

$$\dot{m}_c=\dot{m}_1+\dot{m}_2+\dot{m}_3+\ldots \tag{20}$$

Substituting the value of $\dot{m}_i$ from Equation 19 into Equation 20, we obtain the following expression for the cluster-average values of $f\mathrm{Re}$:

$$\frac{1}{(f\mathrm{Re})_c}=\sum_{i=1}^{n}\left(\frac{A_i}{A_c}\right)\left(\frac{D_{hi}}{D_{hc}}\right)^2\frac{1}{(f\mathrm{Re})_i} \tag{21}$$

Note that the method of superposition is not restricted to laminar or turbulent flow, and is independent of dependence of f on Re.

The cluster-average Nu values were calculated by first determining the average bulk temperature:

$$T^*_{b_c}=\frac{\sum Q_i T^*_{bi}}{\sum Q_i} \tag{22}$$

and heated wall temperature

$$\bar{T}^*_{w_c}=\frac{\sum \bar{T}^*_{wi} P_{hi}}{\sum P_{hi}} \tag{23}$$

Then

$$\mathrm{Nu}_c=\frac{D^*_{hc}}{\bar{T}^*_{w_c}-T^*_{b_c}} \tag{24}$$

for the entire cluster.

Results and discussion

Maximum velocity line

Recall that the location of the MVL was first assumed, heuristically, to be the locus of the point equidistant from both the solid surfaces. This assumption was checked after generating the results for the flow field. The disagreement, if any, was narrowed through iteration. Fortunately, however, the MVL obtained from the converged turbulent solution remained almost unchanged except near the point L, where it shifted marginally towards the shell surface (see Figure 4b). The velocity profile along the MVL (Figure 4a) is also compared with the laminar results.[1] As is expected, the turbulent profile is much more uniform than the laminar value.

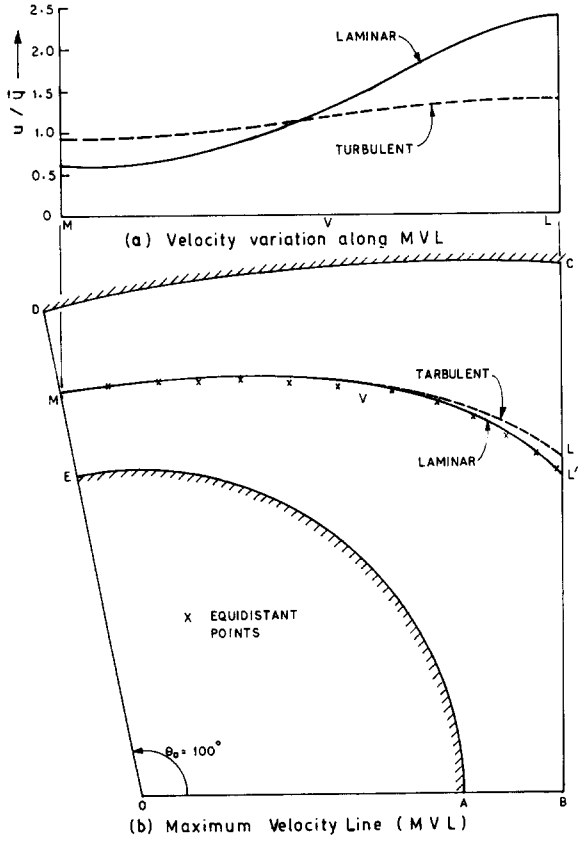

Figure 4 Locus of maximum velocity for a wall subchannel, Type III, $W/D=1.25$, $P/D=1.3$: (a) velocity variation along MVL; (b) maximum velocity line (MVL)

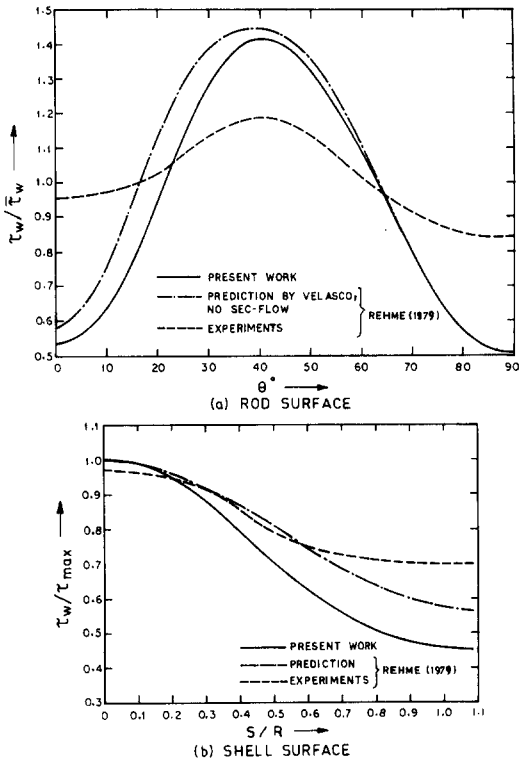

Figure 5 Comparison of wall shear stress distribution, wall subchannel, Type IV, $P/D=W/D=1.071$: (a) rod surface; (b) shell surface

Wall shear stress distribution

The present results for a straight-boundary wall subchannel are compared with experiments and predictions by Rehme,[5] (Figure 5). There is qualitative agreement between the two predictions on the rod surface. The values for the shell surface deviate up to a maximum of 30% near $S/R=1.1$, due possibly to the choice of anisotropy factor made by Rehme. Both the predictions corroborate the trend of the experimental results, but with quantitative deviation. The experimental results are observed to be more uniform for either surface. Comparison of wall shear stress is also made with Seale's predictions, with and without secondary flow (Figure 6a). The distribution on the shell surface is shown in Figure 6b for the same geometry. The wall shear stress distributions for a curved-boundary subchannel are presented in Figure 7. The positions of the maximum and minimum values are located on the shell surface at symmetry points C and D, respectively.

Friction factor

The presently calculated friction factor results were compared with one of the empirical relation developed by Seale[8] for straight-boundary subchannels:

$$f=0.0565/\mathrm{Re}^{0.217} \tag{25}$$

(see Table 1). For subchannel type III, the present values of f are 2 to 3% smaller than the results of Equation 25, over a wide range of Reynolds number varying from 20,000 to 160,000. It is also noted that for almost all cases, the value of the friction factor lies between the two empirical results obtained by the correlations of Blasius and McAdams[26] for smooth pipes. In other words, the friction factor for curved-wall boundary subchannels can be determined with reasonable accuracy by

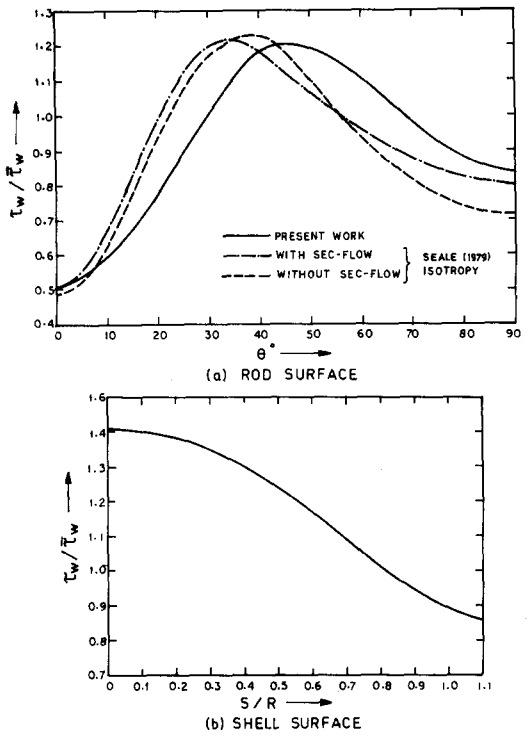

Figure 6 Comparison of wall shear stress distribution, wall subchannel, Type IV, $P/D=1.1$, $W/D=1.185$: (a) rod surface; (b) shell surface

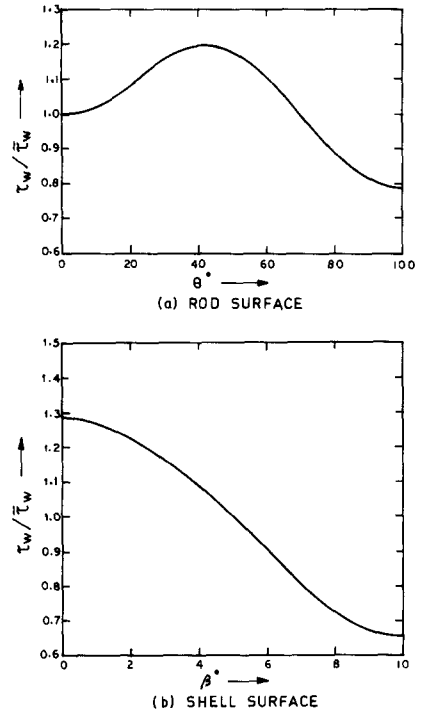

Figure 7 Wall shear stress distribution, wall subchannel, Type III, $P/D=1.3$, $W/D=1.25$, Re=145,000: (a) rod surface; (b) shell surface

the pipe flow correlations, through appropriate use of the concept of hydraulic diameter.

For the straight-boundary subchannels, striking agreements were observed between the presently calculated values of f and those obtained by Equation 25 for higher D_h/R ratios (Table 1b). But with the decrease of the D_h/R ratio, the present values tend to be lower by as much as 10%. Similar trends were marked when compared with the empirical results by McAdams and Blasius.[26] Such variation were also noted by Seale.[8] For a straight-boundary wall subchannel, Rehme[5] determined, by experiments, the friction factor to be $f=0.00454$ for $P/D=W/D=1.07$ at Re=87,300, whereas the present value is 0.00426. For a geometry in which $P/D=W/D=1.15$ and Re=123,000, Slagter[10] obtained $f=0.00438$; the present value at Re=122,800 is 0.00427, and so the agreement is excellent.

The variation of the friction factor with the Reynolds number is shown in Figure 8 for both the curved and straight-wall subchannels; $P/D=1.3$ and $W/D=1.25$. It may be noted that the friction factor for the straight-boundary subchannel is nearly 2% higher than that for the curved wall subchannel.

Temperature variation on rod surface

Computations have been made for the uniform heat flux condition in axial and peripheral directions. Representative variation of temperature on the rod surface is plotted in Figure 9. As expected, the temperature starts from a higher value at $\theta=0°$, decreases steadily in the rod-free zone, and then increases as the gap between the rod and the shell surface narrows down.

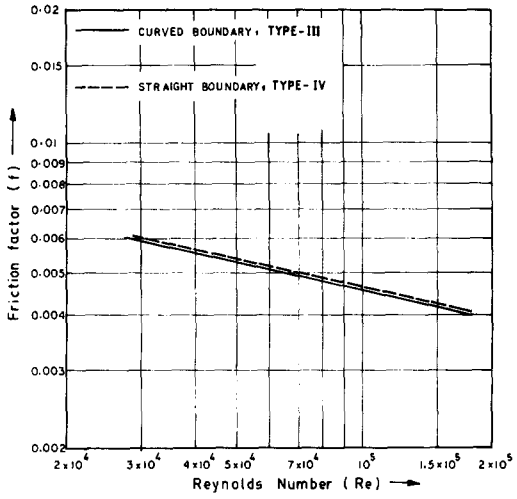

Figure 8 Variation of friction factor with Reynolds number in wall subchannels, $P/D=1.3$, $W/D=1.25$

Table 1 Friction factor results for wall subchannels

Sl. No.	P/D ratio	W/D ratio	θ_0°	Re	Friction factor: Present	Friction factor: Eq. 25
Curved boundary (Type III)						
1.	1.3	1.25	120	159,800	.00411	.00420
2.	1.3	1.25	105	106,100	.00450	.00459
3.	1.3	1.25	105	67,580	.00493	.00506
4.	1.3	1.25	105	30,390	.00589	.00599
5.	1.2	1.15	120	24,370	.00609	.00631
6.	1.2	1.15	105	21,420	.00629	.00649
7.	1.2	1.15	100	20,520	.00641	.00655
Straight boundary (Type IV)						
1.	1.3	1.25	90	80,000	.00483	.00488
2.	1.3	1.25	90	135,000	.00435	.00435
3.	1.2	1.25	90	65,390	.00500	.00509
4.	1.2	1.25	90	122,000	.00440	.00445
5.	1.07	1.07	90	86,200	.00426	.00480
6.	1.15	1.15	90	122,800	.00427	.00444

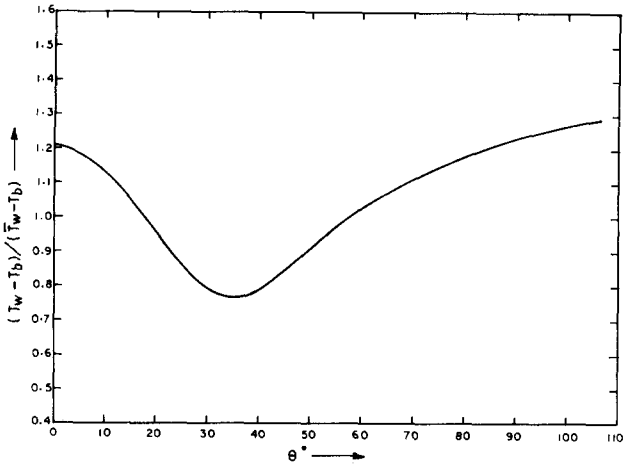

Figure 9 Temperature variation on the rod surface, wall subchannel, Type III, $P/D=1.3$, $W/D=1.5$, 19-rod cluster

Nusselt number

Typical results for the Nusselt number for both curved and straight boundary subchannels are presented in Table 2. The turbulent Prandtl number Pr_t was calculated using Equation 13. In the absence of any literature information, comparison of Nu values was made with the Dittus–Boelter correlation, and the agreement is reasonable. This is contrary to the experience with the interior subchannels.[3] It signifies that the wall subchannels, due to the presence of two solid walls, behave more as an internal geometry than does an interior subchannel.

Cluster-average transport values

The method of superposition is applied to some circular clusters with varying number of rods and geometrical arrangements. The Fanning's friction factor obtained through Equation 21 is compared with the experimental results of Mohanty and Roy[25] (see Table 3). The experimental results are on the average 10% higher than the present values, which may be due to the spacers and end plates used in the experimental setup. Comparison of cluster average values of f with the Blasius[26] correlation indicates that the superimposed values are nearly 5% higher. Based on the above observations, it is recommended that the cluster-average friction factor to be estimated as

$$f=0.083/\mathrm{Re}^{0.25} \tag{26}$$

where Re is estimated using the cluster-average hydraulic diameter.

The average Nusselt number for circular clusters was determined by Equation 24 (see Table 4). Comparison of Nu values with the Dittus–Boelter correlation shows quantitative agreement.

Table 2 Representative temperature solutions for wall subchannels ($Pr=0.7$, Pr_t by the Wassel–Catton model[22])

Sl. No.	P/D ratio	W/D ratio	D_h/R ratio		Re	Nu	
						Present	D–B equation
Curved boundary (Type III)							
1.	1.25	1.25	1.7078	120	35,050	67.781	86.207
2.	1.25	1.25	1.619	105	31,770	68.447	79.694
3.	1.25	1.25	1.5928	100	30,730	68.315	77.583
4.	1.3	1.25	1.6943	105	30,930	69.143	78.002
5.	1.12	1.38	1.9626	120	64,090	136.289	139.701
6.	1.2	1.15	1.2796	120	24,370	60.507	64.447
7.	1.2	1.25	1.542	105	32,920	67.043	81.990
8.	1.2	1.25	1.632	120	36,650	70.956	89.346
Straight boundary (Type IV)							
1.	1.1	1.185	1.0807	90	89,860	192.333	183.068
2.	1.2	1.25	1.4647	90	29,860	80.546	75.821
3.	1.2	1.25	1.4647	90	65,390	147.141	141.956
4.	1.2	1.25	1.4647	90	122,000	199.307	233.865
5.	1.2	1.394	1.9616	90	48,560	115.516	111.889

Table 3 Fanning's friction factor for circular clusters by superposition

Sl. No.	P/D ratio	W/D ratio	No. of rods	Re	Friction factor		
					Present	Ref. 25	Blasius correlation
1.	1.2	1.15	7	22,880	.00635	.00751	.00642
2.	1.25	1.25	7	32,148	.00586	.00690	.00589
3.	1.12	1.38	7	47,351	.00542	.00626	.00535
4.	1.3	1.25	7	155,367	.00423	.00465	.00398
5.	1.2	1.15	19	24,089	.00647	.00741	.00634
6.	1.25	1.25	19	32,450	.00604	.00688	.00588
7.	1.3	1.25	19	165,673	.00424	.00458	.00391
8.	1.2	1.15	37	24,062	.00715	.00741	.00634
9.	1.25	1.25	37	31,917	.00657	.00691	.00591
10.	1.3	1.25	37	167,495	.00455	.00456	.00390

Table 4 Average Nusselt number for circular clusters by superposition (Pr = 0.7, Pr_t by the Wassel–Catton model[22])

Sl. No.	P/D ratio	W/D ratio	No. of rods	D_{hc}/R ratio	Re	Nu	
						Present	D–B equation
1.	1.2	1.15	7	1.250	22,880	59.638	61.281
2.	1.25	1.25	7	1.636	32,148	64.888	80.443
3.	1.3	1.25	7	1.767	155,367	320.875	283.697
4.	1.2	1.25	7	1.506	31,819	65.590	79.784
5.	1.25	1.25	19	1.663	32,450	79.441	81.047
6.	1.2	1.25	19	1.484	30,080	74.349	76.272
7.	1.25	1.25	37	1.692	31,917	85.824	79.982

Conclusions

Turbulent flow and heat transfer through the wall subchannels of circular and hexagonal clusters have been studied numerically by a finite-difference solution. Turbulence has been modeled in two dimensions by a generalization of Reichardt's[20] eddy diffusivity for circular pipes and annuli.

It is observed that the friction factor for a curved-boundary wall subchannel can be reasonably predicted by pipe flow correlations. The pipe correlations can also be applied to straight-boundary wall subchannels, but only at higher values of D_h. For smaller values of D_h, particularly when the shell wall is very close to the peripheral rod, the friction factor decreases from that of the pipe flow and is dependent on the geometry of the subchannel. The Nusselt number for either geometry can be predicted by the Dittus–Boelter correlation with reasonable accuracy.

The transport rate values in a turbulent flow through a finite rod bundle was generated by superimposing the results for the constituent subchannels. The cluster-average values so determined were found to be in good agreement with experimental results in the literature. This leads to a suggestion that the turbulence modeling for a complex geometry may be more conveniently done by considering constituent subchannels.

Whereas the corroborations of transport rate values certify the turbulence model and the computation scheme, the significance of the study lies in the predicted shear stress and rod surface temperature variation. The latter information is pertinent for locating possible hot spots.

References

1 Mohanty, A. K. and Sahoo, K. M. Laminar convection in wall sub-channels and transport rates for finite rod-bundle assemblies by superposition. *Nucl. Eng. Des.*, 1986, **92**, 169–180

2 Shah, R. K. and London, A. L. Laminar flow and forced convection in ducts. *Advances in Heat Transfer*, Supplement I, Academic Press, New York, 1978, 354–365

3 Mohanty, A. K. and Sahoo, K. M. Turbulent flow and heat transfer in rod-bundle sub-channels. *Nucl. Eng. Des.*, 1988, **106**, 327–344

4 Das, R. and Mohanty, A. K. Laminar combined convection in finite circular rod-bundles. *Trans. ASME, J. Heat Transfer*, 1984, **106**, 563–569

5 Rehme, K. The structure of turbulent flow through wall subchannels of rod-bundles. Proceedings, Winter Annual Meeting of ASME, New York, Nov. 1979, 67–76

6 Rehme, K. The structure of turbulent flow through rod bundles. *Nucl. Eng. Des.*, 1987, **99**, 141–154

7 Seale, W. J. Turbulent diffusion of heat between connected flow passages, Part 1: Outline of the problem and experimental investigation. *Nucl. Eng. Des.*, 1979, **54**, 183–195

8 Seale, W. J. Turbulent diffusion of heat between connected flow passages, Part 2: Prediction using K- turbulence model. *Nucl. Eng. Des.*, 1979, **54**, 197–209

9 Seale, W. J. Measurements and predictions of fully developed turbulent flow in a simulated rod bundle. *J. Fluid Mech.*, 1982, **123**, 399–423

10 Slagter, W. Finite element solution of axial turbulent flow in a bare rod bundle using a one-equation turbulence model. *Nucl. Sci. Eng.*, 1982, **82**, 243–259

11 Ramm, H. and Hohannsen, K. A phenomenological turbulence model and application to heat transport in infinite rod arrays with axial turbulent flow. *Trans. ASME, J. Heat Transfer*, 1975, **97**, 231–237

12 Meyder, R. Turbulent velocity and temperature distribution in the central subchannel of rod bundles. *Nucl. Eng. Des.*, 1975, **35**, 181–189

13 Thompson, J. J. and Holy, Z. J. Conjugate heat transfer and thermoelastic analysis of heat generating rods. *Nucl. Eng. Des.*, 1975, **35**, 247–268

14 Carajilescov, P. and Todreas, N. E. Experimental and analytical study of axial turbulent flow in an interior sub-channel of a bare rod bundle. *Trans. ASME, J. Heat Transfer*, 1976, **98**, 262–268

15 Trupp, A. C. and Aly, A. M. M. Predicted secondary flows in triangular array rod bundles. *Trans. ASME, J. Fluids Eng.*, 1979, **101**, 354–362

16 Bartzis, J. G. and Todreas, N. E. Turbulence modelling of axial flow in bare rod bundles. *Trans. ASME, J. Heat Transfer*, 1979, **101**, 628–634

17 Rehme, K. The structure of turbulent flow through a wall sub-channel of a rod-bundle. *Nucl. Eng. Des.*, 1978, **45**, 311–323

18 Rapley, C. W. The calculation of local mean flow characteristics in turbulent fully developed rod bundle passage flows. *Proc. 4th GAMM-Conf. Num. Meth. Fluid Mech.*, 1982, **5**, 272–280

19 Sahoo, K. M. Numerical prediction of energy and momentum transport in finite rod-bundles. Ph.D. thesis submitted to Indian Institute of Technology, Kharagpur, 1987

20 Levy, S. Turbulent flow in an annulus. *Trans. ASME, J. Heat Transfer*, 1967, **89**, 25–32

21 Jayatilleke, C. V. L. The influence of Prandtl number and surface roughness on the resistance of the laminar sublayer to momentum and heat transfer. *Progress in Heat Mass Transfer*, Vol. 1 (U. Grigull and E. Hanse, Eds.), Pergamon Press, London, 1969

22 Wassel, A. T. and Catton, J. Calculation of turbulent boundary layers over flat plates with different phenomenological theories of turbulence and variable turbulent Prandtl number. *Int. J. Heat Mass Transfer*, 1973, **16**, 1457–1563

23 Brighton, J. A. and Jones, J. B. Fully developed turbulent flow in annuli. *Trans. ASME, J. Basic Eng.*, 1984, **86**, 835–842

24 Kaiser, H. G. and Zeggel, W. Turbulent flows in complex rod bundle geometries, numerically predicted by the use of FEM and a basic turbulence model. *Nucl. Eng. Des.*, 1987, **99**, 351–363

25 Mohanty, A. K. and Roy, D. K. Fluid flow through a circular tube containing rod clusters. *Fluid Flow and Heat Transfer Over Rod or Tube Bundles*. ASME, Winter Annual Meeting, New York, Nov. 1979, 121–128

26 Rohsonow, W. M., Hartnett, J. P. and Ganić, E. N. *Handbook of Heat Transfer Fundamentals*. 2nd ed. McGraw-Hill, New York, 1985